Experimental Validation of Active Filter Functionality for Distributed Photovoltaic Farms

Grazia Todeschini, *Senior Member, IEEE,* Atheer Habash,
Jacob Lynch, and Zia Emin, *Senior Member, IEEE*

***Abstract*—Power electronics-interfaced devices, including photovoltaic panels, wind generators and energy storage, are being installed at fast pace across the electrical grid. Their control system can be programmed to perform a variety of ancillary services. Assessment of these features and their impact on power system operation requires detailed simulations and experimental validation.**

This paper aims at presenting and verifying a control strategy where PV inverters are used as active filters. The innovative aspects of the proposed approach are: the use of detailed network data to represent the behaviour of the inverter under real operating conditions, the design of control features to ensure that inverter and transformer ratings are not exceeded, and the assessment of using different measurement points to detect harmonic currents. The paper presents the structure of the proposed algorithm, simulation results, and the steps undertaken to carry out the experimental validation.

***Index Terms*—Active filter (AF), power electronics-interfaced device (PEID), total harmonic distortion (THD), hardware-in-the-loop (HIL).**

I. Introduction

INTEGRATION of power electronics-interfaced devices (PEIDs) in the distribution system is rapidly growing in the form of both generation and loads. Examples of PEIDs include photovoltaic (PV) panels and electric vehicles (EVs). Individual installations must comply with network performance requirements, such as harmonic distortion levels [1]–[3]. However, a combination of a large number of PEIDs connected in close proximity may result in an overall increase in harmonic distortion in the distribution system [4], [5]. Although harmonic distortion may not visibly affect power system operation, it may compound already existing thermal constraints on the network. As a result, network owners and operators seek methods to mitigate some of these adverse impacts.

Historically, passive shunt filters have acted as a sink for harmonic currents, offering a low impedance route for specific frequencies [6]. A more recent approach gaining traction is active filtering, which uses a power converter to produce harmonic currents that neutralize those within the network [7]. This functionality can be performed by a specialized device such as a STATCOM. Alternatively, it can be provided by PEIDs as an ancillary service. This is an attractive opportunity that allows for more effective utilization of exiting grid assets, with limited expenditure, while improving grid operation [8].

To quantify the impact of advanced control features on the power system, advanced power system studies are required. Traditionally, harmonic assessment has been carried out using frequency-domain studies, due to the steady-state nature and well-known characteristics of harmonic injection [4].

Assessing the influence of control mechanisms on the power system, especially under time-varying operational scenarios, necessitates the use of electromagnetic transient (EMT) studies. EMT studies are more complex than frequency domain or rms studies, because they require detailed modeling of PEID and are more computationally demanding. Nevertheless, this approach is growing in popularity, and TSOs and DNOs worldwide are developing EMT models of their systems to capture the more complex dynamic behavior of the electrical system with increasing PEIDs.

EMT studies involving PEIDs are followed by hardware-in-the-loop (HIL) testing. In general terms, HIL refers to the condition in which the control algorithm is deployed on a microcontroller, that is interfaced with a digital simulator through analog and digital signals [9]. The digital simulator is a device that allows emulating the actual power grid in real-time operating conditions, including interactions with the microcontroller. This approach has been used for power system studies at both the transmission and distribution system level [9]–[11]. Power HIL (PHIL) is a further enhancement of this concept, where power is exchanged between the power converter and the real-time digital simulator (or alternatively, the grid) [12]. Both PHIL and HIL main requirement is the ability to run in real time, as the microcontroller duplicates PEID simulation and needs a high sampling frequency.

The use of a EV charging station to act as AF is studied in [13]. The proposed design is based on the use of a Kalman filter and proportional-resonant (PR) controllers, as the authors observe that PI controllers are mostly effective at fundamental current. The paper demonstrates the effectiveness of this apporach using both EMT and HIL studies, and in particular demonstrate the achievement of a constant dc bus voltage. A similar concept is presented in [14], where AF operation is performed during both EV charging and discharging. Simulation results show the effectiveness of the proposed method, however, only a simplified version of the control algorithm is described in the paper and experimental studies are not carried out.

Due to the intermittency of solar radiation [15], PV farms have a large capacity to provide ancillary services, including

G. Todeschini is with the Department of Engineering, King's College London (grazia.todeschini@kcl.ac.uk); A. Habash is with GE Vernova (atheer.habash@ge.com), J. Lynch is with National Grid Electricity Distribution (jlynch@nationalgrid.co.uk), Z. Emin is with Electric Power Research Institute (zemin@epri.com).

Manuscript received XXXX; revised XXXX.

harmonic mitigation. The Authors of [16] present a control methodology applied to active filters, where a comb filter is integrated into the SOGI-PLL. Experimental validation demonstrates that this approach is effective, but the comb filter is computationally expensive.

In summary, the literature review demonstrated that the provision of AF functionality from PEIDs is effective, but the works on this topic do not address the use of different points for reference current measurements and do not discuss in detail measures to ensure that inverter and transformer ratings are not exceeded. This paper addresses both these aspects. Additionally, since one of the assumptions of this work was to retrofit existing PV inverters to provide this functionality, design constrains needed to be taken into account.

This paper presents some results for an innovation project led by National Grid Electricity Distributor (formerly, Western Power Distribution), the largest UK distribution network operator (DNO). This project aimed at comprehensively studying the use of PV inverters as Active Filters (AFs) in a portion of their distribution system. Previous papers from this project presented some results, in particular a description of the earlier version of the algorithm, and some of the simulation results [17], [18]. This paper presents the final version of the control algorithm, demonstrates that the algorithm is effective under several operating conditions while ensuring that inverter and transformer ratings are not exceeded, and simultaneous operation across numerous PV farms. Both numerical and experimental validation are presented.

Section II briefly outlines the methodology, while Section III presents the proposed control. Section IV describes the distribution system under consideration and network model. Validation of the proposed algorithm via simulations is illustrated in Section V, while Section VI presents the experimental results. Conclusions are included in Section VII.

II. Methodology

The methodology adopted for this study consisted of the following main steps:

Development of the control algorithm for AF operation: The AF algorithm detects harmonic currents in the grid and allows regulating the PV inverter switching to inject harmonic currents in counterphase to achieve harmonic cancellation. Continuous refinements of the algorithm were carried out during computational and experimental validation.

Model of the network: a detailed distribution system model was built for EMT studies in Simulink. SCADA measurements (with 30 minute resolution) and harmonic measurements (with 10 second resolution) were included into the model. The observation period corresponded to a period of 19 days of real system data collected in October 2019. Load flow and harmonic studies were used to validate the network model against data provided by NGED.

Numerical validation of the proposed algorithm: simulations were carried out to demonstrate the impact of the control algorithm on harmonic levels. The algorithm was initially developed and tested on an individual inverter, it was then deployed on multiple inverters where each device was controlled independently. Finally, coordination between the inverters was studied, with the aim of distributing harmonic compensation duties between different devices.

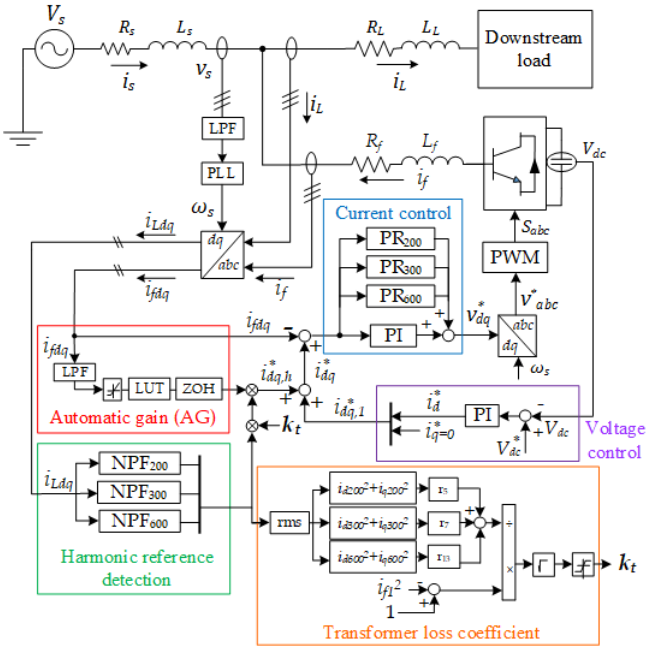

Fig. 1: Overview of the control algorithm including fundamental and harmonic current regulation. The inverter transformer is not shown for simplicity.

Experimental validation of the proposed algorithm: HIL studies were carried out to duplicate the results carried out in simulation and provide further verification of the proposed algorithm.

III. Control Algorithm Development

In this study, the primary control function of the PV inverter is to deliver fundamental power, with AF operation being treated as an ancillary service. [8]. As a result, fundamental power delivery takes priority and AF operation is performed under controlled conditions. Existing PV farms (described in Section IV) were considered to provide AF functionality. The inverters installed at the PV farms are from various manufacturers, and detailed information on their control structure was not available. Therefore, a typical control algorithm used in PV farms was designed for fundamental power regulation, briefly described in the next section.

A. Fundamental current regulation

The fundamental current algorithm includes a maximum point of power tracking (MPPT), a phase-locked loop (PLL), an outer voltage loop, an inner current loop, and a pulse-width modulator (PWM). Figure 1 shows these blocks with the exception of the MPPT, to reduce the complexity of the diagram [17], [18]. Four quantities are fed to the controller: three-phase grid voltage (v_s), inverter dc voltage (V_{dc}), three-phase load current (i_L), and three-phase filter current (i_f). The load current is used to extract the harmonic reference currents

used by the AF algorithm, as will be explained in the next section.

The grid voltage is passed through a low-pass filter (LPF), to remove harmonic components above the fundamental. Once filtered, the voltage is fed to a PLL that calculates the rotating frequency ω_s, used to perform the dq transformation. For the outer voltage loop, a standard dc voltage regulator is adopted, where the d-axis fundamental frequency reference current i_d^* is calculated from the solar irradiance and dc reference voltage. The q-axis reference current is equal to zero ($i_q^* = 0$), since unity power factor is assumed at the inverter terminals. The reference signal (i_{dq}^*) fed to the current loop is the sum of fundamental ($i_{dq,1}^*$) and harmonic components ($i_{dq,h}^*$). A proportional integral (PI) regulator is used for the regulation of fundamental current components. As will be explained in the next section, proportional-resonant controllers (PR) will be used to regulate the harmonic components. The output of the current regulator is the voltage reference v_{dq}^*, that is then used to generate the switching signals S_{abc}.

B. Harmonic current regulation

The harmonic reference harmonic currents are derived from the harmonic current components circulating within the electrical network. The current signal employed to extract these harmonic components is denoted as i_L in Fig. 1 and it corresponds to the current supplying a downstream load. (Various measurement points for i_L can be utilized, each having different effects on the harmonic current algorithm's efficiency, as will be demonstrated later). The current i_L is converted into the dq domain, adopting the same reference frame as the other quantities used by the controller. The harmonic components are then extracted through the use of three notch-peak filters (NPFs). As indicated in the literature, the PI regulator cannot regulate harmonic components with zero steady-state error due to bandwidth constraints [13], [20], [21]. Consequently, three proportional-resonant (PR) controllers were employed.

The number of NPFs, PR controllers, and their calibration depend on the properties of harmonic distortion in the region where the algorithm operates. A greater number of filters would enhance the algorithm's performance, albeit with increased complexity. For the distribution system under evaluation, power quality assessments indicated that the primary harmonic components present were the 5$^{\text{th}}$, 7$^{\text{th}}$, 11$^{\text{th}}$, and 13$^{\text{th}}$. No sequence data could be extracted from the measurements, though this point is crucial because the sequence order impacts the frequency of the current components in the dq domain, and thus the tuning of the resonant filters. Therefore, to assess the resilience of the proposed method, the response to both negative- and positive-sequence 5$^{\text{th}}$ harmonic components was analyzed. The conventional sequence order was used for the other harmonics, namely positive-sequence 7$^{\text{th}}$ and 13$^{\text{th}}$, and negative-sequence 11$^{\text{th}}$ [6]. Upon transforming these harmonics from the abc frame to the dq frame, three frequencies are derived: 200 Hz (from the positive sequence 5$^{\text{th}}$ harmonic), 300 Hz (from the negative-sequence 5$^{\text{th}}$ and positive-sequence 7$^{\text{th}}$), and 600 Hz (positive-sequence 11$^{\text{th}}$, and negative-sequence 13$^{\text{th}}$). Hence, the R controllers were tuned to these frequencies: 200 Hz, 300 Hz, and 600 Hz. Next, the outputs of the PR controller were added to the output of the PI controller used to regulate fundamental frequency, to obtain the voltage reference signals.

C. Harmonic current curtailment

AF duties were distributed among several converters installed at each PV farm. Nevertheless, under specific operational scenarios, AF activity could potentially exceed the inverter's rated capacity. Such scenarios might correspond to high fundamental current output from the inverter, or high system harmonic currents. To safeguard the inverter and transformer from excessive harmonic current contribution, two control functions were developed for the aforementioned conditions. The first function is known as 'automatic gain' (AG) [17], and the second is referred to as 'transformer loss coefficient' [18].

1) Automatic gain (AG): AG is a multiplication factor that can take a value between 0 and 1, and modulates the harmonic current reference. Specifically, when AG equals 0, the harmonic reference currents fed to the downstream controller are nil, and on the other extreme, when AG equals 1, the harmonic reference currents are fed unaltered to the resonant controllers. The AG value is derived by following the procedure illustrated in Fig. 1: the current i_{fdq} is filtered to extract the fundamental component, and this value is used as input to a lookup table to determine the AG value. A lookup table was used because the relationship between AG and fundamental current is non-linear [18]. A zero-order hold (ZOH) was added to ensure that the value of the AG did not change too quickly, thus resulting in excessive swings of harmonic injection during transient conditions (for example, due to passing clouds). As a result, the ZOH allows the AG to update every 10 min (33 ms in simulation).

2) Transformer loss coefficient k_t: When the AF function is enabled, the step-up transformer linked to the inverter might experience losses surpassing the rated values, even after the modulation introduced by the AG. This occurs because harmonic losses in the transformer are proportional to the square of the harmonic current and the equivalent resistance of the transformer increases with frequency. [22]. Excessive harmonic losses may lead to a shortening of the life of the transformer, and should be avoided. A transformer loss coefficient (k_t) was designed to reduce harmonic current injections if they result in transformer losses exceeding the rated value [18]. The expression of k_t is obtained from the standard formulation of power losses p_{Cu}, as follows:

$$p_{Cu} = \sum_h r_h i_h^2 \tag{1}$$

where all quantities are expressed in per-unit and h is the order of the harmonic currents flowing through the transformer, with h = 1, 5, 7, 11, 13. In this instance, i_h is used to maintain simplicity of the notation and maintain generality.

The same coefficient k_t is applied for all harmonic current components, but not for the fundamental. This approach was chosen by observing that, while the lower harmonic orders

have generally larger magnitude, the higher harmonics are associated to increasing equivalent resistance. Applying the constraint that transformer losses must be below the rated value ($p_{Cu} \leq 1$), (1) can be written as:

$$\left(p_{Cu} = r_1 i_1^2 + k_t \sum_{h=5,7,11,13} r_h i_h^2 \right) \leq 1 \tag{2}$$

and therefore the transformer loss coefficient is calculated as follows:

$$k_t \leq \frac{1 - i_1^2}{i_5^2 r_5 + i_7^2 r_7 + i_{11}^2 r_{11} + i_{13}^2 r_{13}} \tag{3}$$

where r_5, r_7, r_{11} and r_{13} are the (per unit) frequency-dependent transformer resistances calculated according to [22]. Expression (3) is rewritten in the dq frame and for the system under study as follows, using the notation of Fig. 1) [1]:

$$k_t \leq \frac{1 - i_{f1}^2}{(i_{dq,200}^2) r_5 + (i_{dq,300}^2) r_7 + (i_{dq,600}^2) r_{13}} \tag{4}$$

where i_{f1} refers to the fundamental current of i_{fdq}.

The coefficient calculated according to (4) results in very high values when the harmonic components are close to zero - due to the division term. In contrast, it is close to zero for high harmonic current values detected during high-irradiance conditions, thus limiting excessively the injection of harmonics. Therefore, lower and upper thresholds were introduced to control the value of k_t to be between 0.3 and 5. In this way, the coefficient acts to protect the transformer losses but does not interfere with the fast regulation provided by the algorithm, and extremely high values due to the division term are not allowed.

The tuning of k_t should be performed for each specific application, as it depends on factors such as transformer rating, transformer equivalent impedance, and harmonic levels in the system, for instance. For the case of the system under study, the impact of the lower threshold was observed to be more evident in at one of the PV farms. Following tests, it was concluded that the use of the same parameters for all locations was a good compromise between simplicity of implementation and effectiveness of the algorithm.

IV. Tiverton Network Model

The proposed functionality was initially deployed using simulation studies, based on the model of a real network located in South-West England. Figure 2 illustrates the single-line diagram of the distribution network, the location of the loads, and of the PV farms.

NGED supplied a DIgSILENT PowerFactory (DPF) model of the network, which was subsequently converted to MATLAB/Simulink. Wherever feasible, the identical network components used in DPF were adopted in Simulink. For instance, all feeders were modelled using distributed parameters, and

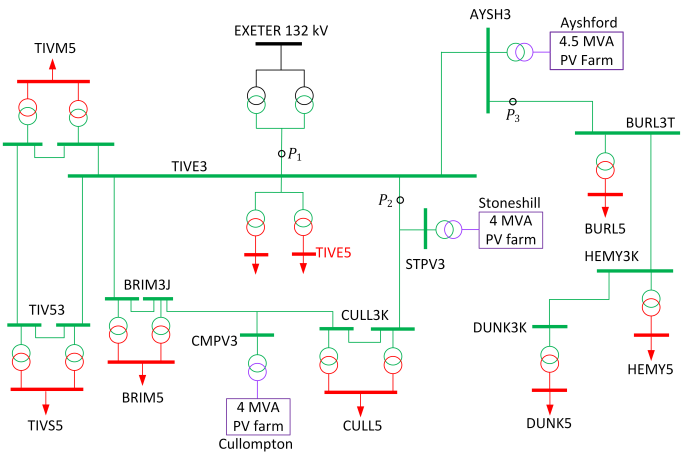

Fig. 2: Single-line diagram of the distribution network under consideration.

TABLE I: Inverter parameters.

Parameter	Ayshford	Stoneshill	Cullompton
Inverter rated power	500 kVA	800 kVA	1800 kVA
Inverter rated voltage	400 V	380 V	400 V
Total export capacity	4.5 MVA	4 MVA	4 MVA

TABLE II: Main controller parameters.

	PI	PR_{200}	PR_{300}	PR_{600}
K_p	0.2	0.3	0.3	0.8
K_i	2.4	120	120	300

the upstream network model included a frequency-dependent equivalent impedance. Owing to the short feeders and the utilization of distributed parameters for line modeling, the simulation sampling time was set to 8 μs [23]. All feeders possess a rated voltage of 33 kV, and eight loads are connected to the network via 33/11 kV transformers. TIVE3 is the main busbar and is supplied from the 132 kV network through two parallel transformers. Three PV farms are connected to the 33 kV network: Ayshford, Stoneshill, and Cullompton. A summary of the inverter ratings for each PV farm is presented in Table I, while Table II details the controller parameters. The reports available on the project website offer further details on the network model [19][2].

In addition to the network model, NGED provided two sets of measurement data for 19 days in October 2019. The first set included of SCADA recordings of system voltage, active (P), and reactive (Q) power with a resolution of 30 minutes at all busbars shown in Fig. 2. The second set consisted of power quality measurements (harmonic currents and voltages) at TIVE3 and at the PV farms, recorded with a higher resolution of 10 s. Power quality (PQ) data was used to accurately model PV generation, as the high resolution allowed the rapid fluctuations of irradiance to be duplicated.

[1]The expression below and Fig 1 do not include r_{11}: this resistance is combined with r_{13} to simplify the formulation, while resulting in a slightly conservative calculation for k_t.

[2]Readers interested in detailed network parameters are advised to request this information to NGED by sending an email to nged.innovation@nationalgrid.co.uk.

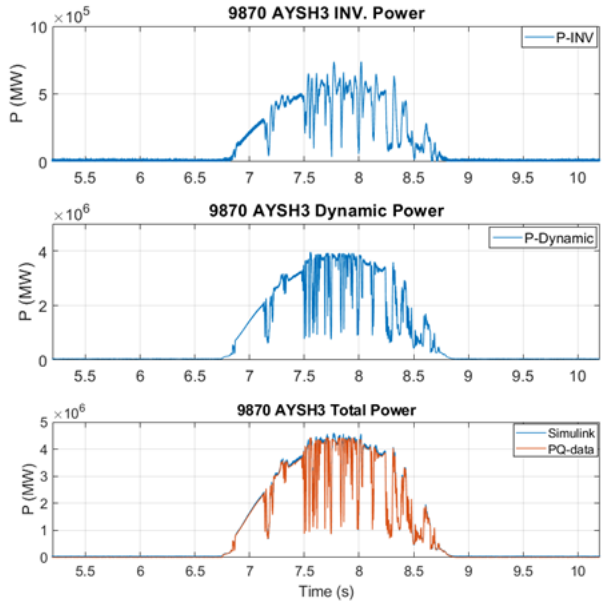

Fig. 3: Ayshford PV farm power output: top - individual inverter, middle - dynamic model, and bottom: total power output and comparison with measurement.

TABLE III: Individual harmonics and THD values (%) from measurement data and simulation.

	Measured data			Simulation		
Harmonic	V_{12}	V_{23}	V_{31}	V_{12}	V_{23}	V_{31}
5	1.32	1.40	1.40	1.31	1.31	1.31
7	1.10	1.06	1.09	1.04	1.04	1.04
11	0.21	0.28	0.26	0.26	0.26	0.26
13	0.22	0.28	0.26	0.28	0.28	0.28
THD	1.60	1.67	1.55	1.73	1.73	1.73

A. Harmonic sources

Three sources of harmonic distortion were identified: loads on the 11 kV buses, PV farms, and upstream distortion from the 132 kV network. Since harmonic measurements were taken at only four locations, several assumptions were made based on engineering knowledge of the network and best practices to model these sources. The harmonics produced by the 11 kV loads were considered to be proportional to the fundamental current, which was obtained from SCADA data. Given the high quantity of PEIDs in the network, the PV farms were modeled as a combination of a detailed inverter model and an equivalent PV dynamic model with current sources. The harmonic current sources at the PV farms were calibrated to match the measurements from the PQ data. The background harmonic distortion at the 132 kV busbar was modeled with four harmonic voltage sources at the frequencies of interest (5^{th}, 7^{th}, 11^{th}, and 13^{th}), connected in parallel and series with the system frequency-dependent impedance. According to typical engineering practice, it was assumed that upstream distortion contributes to 10% of the voltage THD measured at TIVE3, and the amplitude of each upstream voltage source was adjusted as needed. The harmonic injection at both the load and the source was calibrated to ensure that the voltage distortion at TIVE3 predicted by the simulation matched the measurements taken over the 19-day observation period.

B. Model validation

The Simulink model was verified with the data supplied by NGED through load flow, contingency, and harmonic studies. Some outcomes, such as load flow analysis and frequency scans, were also benchmarked against the original DPF model. Comprehensive details are available in the reports cited at [19], while this section presents a subset of the results. Concerning time-domain and fundamental power validation, Fig. 3 illustrates the power output at the Ayshford PV farm. As described in the previous paragrah, the PV farm model incorporates an inverter and a PV dynamic model. The output from these two components is shown in the first and second graphs, respectively, while the overall output power for Ayshford PV is depicted in the final graph. This curve is exactly in alignment with the 10-second measurement (PQ data).

Harmonic studies were conducted to assess the performance of the model against the measurement data. For the sake of brevity, this paper exemplifies the comparison in terms of both individual harmonic components and total harmonic distortion (THD) calculated at the TIVE3 busbar. Table III presents THD average values caclulated throughout the monitoring period. In general, the harmonic components are quite similar across the three phases. The measured data show some imbalance; however, since the cause of the imbalance could not be identified from the available data, a symmetrical system was modeled, which shows good agreement.

V. Numerical validation of the AF functionality

The control algorithm described in Section III was tested under a variety of operational scenarios, including contingency cases. First, the algorithm was implemented at Ayshord PV farm, and later at the three PV farms connected to the Tiverton Network [17], [18]. This section will presents results with respects to three aspects: performance for an individual PV farm, evaluation of various measurement locations, and simultaneous operation across PV farms.

A. Performance of the algorithm for one PV farm

Initially, the performance of the algorithm, including AG and k_t, were tested at the Ayshford PV farm.

Figure 4 shows time-domain results for two typical operating conditions: low irradiance and high irradiance. The first graph shows fundamental rms current against the rated value, the second shows the harmonic gain (AG) and the last figure the time domain current, including both fundamental and harmonic components. The inverter rating is never exceeded under any operating conditions. These results were verified across the entire simulation range.

Fig. 5 presents the copper losses for the Ayshford PV farm transformer with the aim to assess the effectiveness of k_t. These losses are calculated according to (1). The first graph shows losses due to harmonic currents, the second graph shows

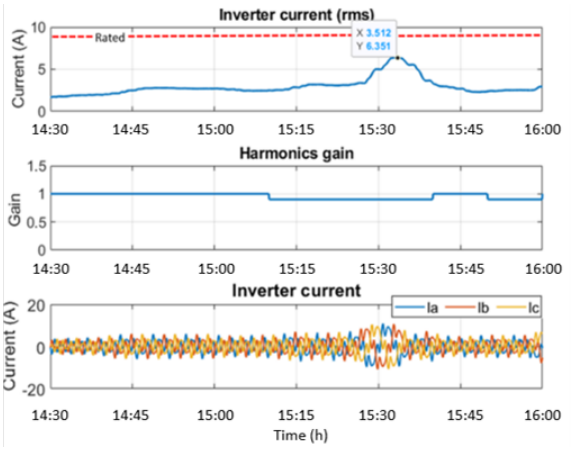

(a)

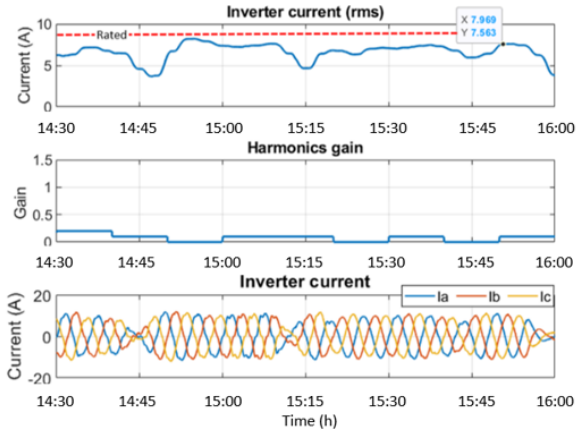

(b)

Fig. 4: Inverter current with different values of irradiance: (a) low irradiance and (b) high irradiance.

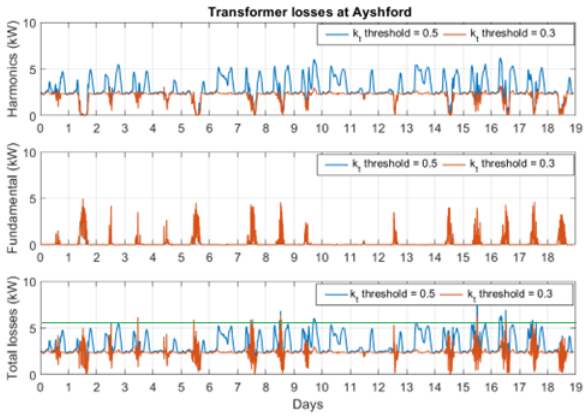

Fig. 5: Transformer losses at Ayshford for two values of the transformer loss coefficient: losses due to harmonic components, losses due to fundamental current, and total losses.

those due to fundamental current, and the third graph shows the total. The rated transformer losses are 5.4 kW and are indicated by a horizontal line. The results are displayed for two different values of the coefficient k_t lower threshold. With

TABLE IV: Current measurement point for each PV farm

Case	Ayshford	Stoneshill	Cullompton
1	P_3	P_1	P_1
2	P_1	P_2	P_1
3	P_3	P_1	P_1

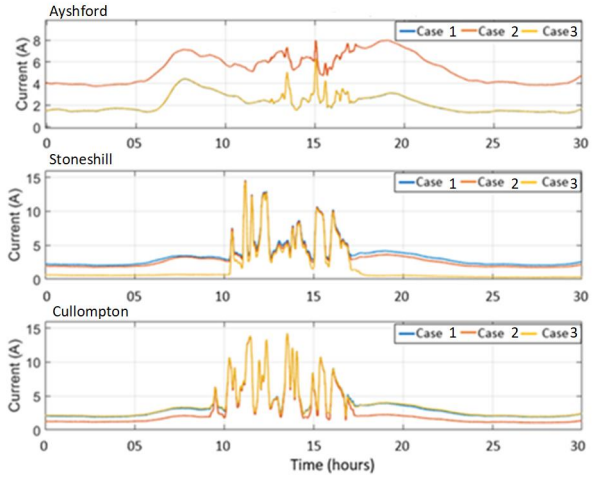

Fig. 6: Inverter rms currents for the cases shown in Table IV.

a lower threshold equal to 0.5, harmonic injection causes significant power loss, approaching the transformer rated value. When the lower threshold is 0.5, the harmonic losses drop considerably. As shown in the second graph, the fundamental power losses remain unaffected by k_t, since this coefficient impacts only harmonic components. The third graph shows that a lower threshold value leads to reduced overall losses, however this choice reduces significantly the effectiveness of the AF functionality. Thus, this analysis underscores the necessity of precise coefficient tuning. For subsequent studies, a lower threshold equal to 0.3 was used.

B. Evaluation of alternative current measurement locations

In [18], AF operation was deployed in the three PV farms depicted in Fig. 2, where the downstream feeder current (denoted as i_L in Fig. 1) was employed to determine the harmonic currents. This section aims to discuss whether utilizing alternative measurement points would result in more efficient harmonic mitigation. This hypothesis was tested by selecting eight different measurement points to supply the current i_L to the inverters at the PV farms. These points corresponded to busbars equipped with measurement relays. Ideal synchronization between measurements was assumed, and it was also decided to maintain a consistent measurement point throughout the entire simulation period [19]. From these initial tests, three locations were identified as yielding the best harmonic mitigation, and are denoted as P_1, P_2, and P_3 in Fig. 2. The three most significant scenarios are presented in Table IV, where for each PV farm, a distinct measurement point for the current i_L was utilized.

The inverter rms current for each case is depicted in Fig. 6 over the initial 30 hours of the observation period. The initial graph in Fig. 6 displays the Ayshford rms current (including

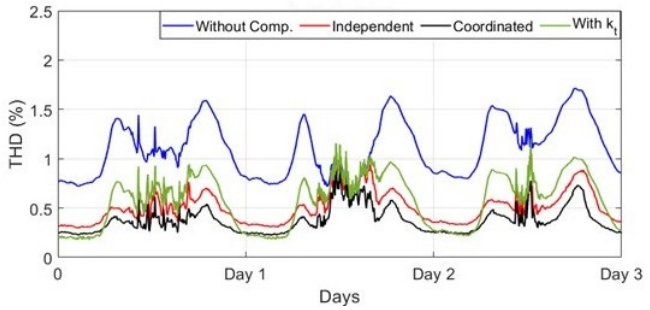

Fig. 7: Voltage THD at TIVE3 for the original case, and the three operating conditions studied above.

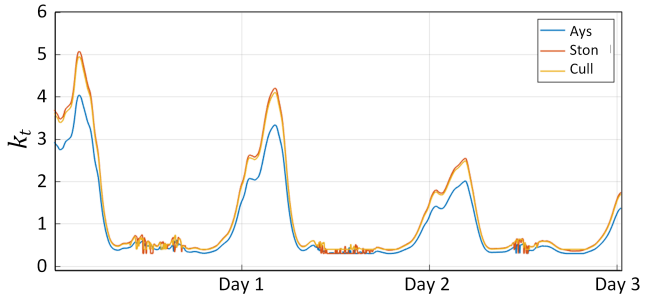

Fig. 8: Transformer loss coefficient at all sites.

both fundamental and harmonic components): for this inverter, the current in Case 1 and Case 3 is the same since the measurement point (P_3) is adopted. The current for Case 2 (using P_1) is significantly higher. This result is explained by observing that, when P_1 is utilized, the harmonic reference is computed using the total current delivered to the loads, and therefore Ayshford undertakes more harmonic compensation. In contrast, when P_3 is used, only the harmonic currents generated by the loads connected to the radial feeder are considered.

The second graph in Fig. 6 shows the rms current at Stoneshill: Case 1 and Case 3 use P_1 and result in the highest harmonic current injection, while for Case 2, adopting P_2, the current is lower. As observed in Ayshford, this result can be explained by noting that P_1 results in a higher harmonic reference current for the inverter at Stoneshill.

The third graph in Fig. 6 portrays the rms current at Cullompton: even though P_1 is consistently used across all cases, the inverter current varies. This variation can be explained by noting that, in Case 1, Ayshford assumes more harmonic compensation tasks, thus reducing the harmonic content included in P_1 and consequently lowering the harmonic reference current for the Cullompton inverters.

The above tests demonstrate that PV farms can compensate for harmonic currents generated anywhere in the system, rather than just by the downstream loads. Since the algorithm developed includes features to limit harmonic current injections (AG and k_t), it is concluded that the most effective approach is to adopt the measurement point where the highest harmonic currents can be detected, thus maximizing the impact of AF operation.

C. Simultaneous operation across PV farms

The overall impact of the algorithm was assessed by monitoring voltage THD at TIVE3 for various conditions. The results for four cases are discussed in details in this section:

- Results for the original system, with no harmonic mitigation applied (Without Comp.)
- The PV farms operate independently, with measurements point set to P_1 for Stoneshill and Cullompton and set to P_3 for Ayshford (Independent)
- The PV farms operate in a coordinated way, with the feedback load current measurements point set to P_1 for all inverters (Coordinated)
- The PV farms operate in a coordinated way, with the feedback load current measurement point set to P_1 for all inverters with the transformer loss coefficient included and equal to 0.3 (With k_t).

Figure 7 depicts the voltage THD at TIVE3 for the four aforementioned cases over the first three days of the observation period. These results are representative of the entire observation period and are presented for clarity. The THD pattern repeats similarly each day, being lower during the daytime and higher at night. This characteristic, noted in other studies [24], further supports the proposed algorithm, since during nighttime the PV panels have a greater capacity for harmonic mitigation, when this functionality is more needed.

Although all tests result in a reduction of harmonic levels in the system, it is pertinent to mention that at noon on Day 2, all curves coincide with the original data, showing no THD improvement. Upon closer examination, this is attributed to high PV generation at all PV farms, which causes the inverters to not inject harmonics. These results demonstrate that the AG functions as intended. Overall, the optimum result occurs with coordinated operation, noted as 'Coordinated'. As anticipated, the inclusion of k_t diminishes the algorithm's performance, resulting in reduced harmonic compensation.

Further insights on the last test (With k_t) are provided in Fig 8, where k_t is plotted as a time series for the same period as Fig. 7 During the nigh, k_t reaches high values because the inverter fundamental current is low, while during the day harmonic injection is limited. The figures shows k_t for the three PV farms, indicating a similar trend, but different values, due to diversity in irradiance and harmonic injection at each farm.

VI. Experimental validation

The experimental setup for this work includes an OPAL-RT 5600 emulator and a PELab power converter. These devices are connected via DB27 ports for exchanging analog and digital signals, and conducting HIL studies. The OPAL-RT is linked to a laptop through an Ethernet cable, while the PELab is connected using a USB-to-USB cable. Two oscilloscopes are used to measure the three-phase voltage waveforms at the inverter terminals and within the TIVE3 network. Figure 9 shows the experimental setup and the connection between various components.

The PELab was used to emulate the operation of the Ayshford inverter, while the rest of the system was programmed in the digital simulator.

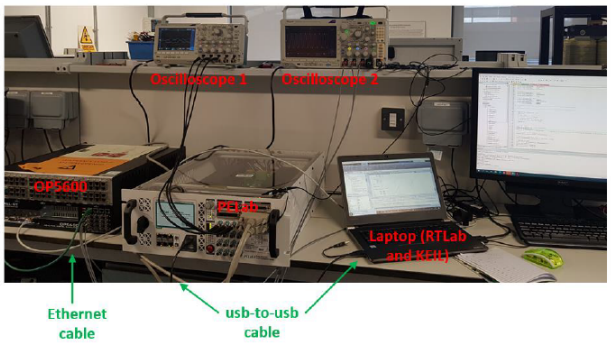

Fig. 9: Set up of the experimental test bench.

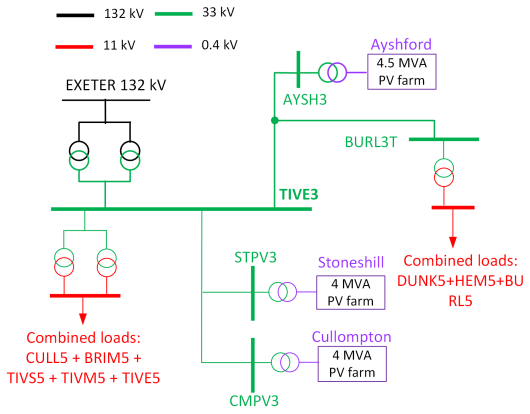

Fig. 10: Reduced network model

.

RT-LAB serves as the software platform for programming the real-time simulator, and is fully integrated with MATLAB/Simulink. This allowed using the same model used in simulation for real-time testing. To enable hardware integration, certain components such as digital and analog inputs/outputs need to be incorporated into the model. MATLAB version 2019b along with RT-LAB 2020.1 were utilized.

The control system was converted into C to be used by the microcontroller. The PE-LAB is equipped with two microcontrollers, the ST Microelectronics ARM® Cortex® M7 and M4 dual-core STM32H745BI. For the experimental work presented here, only one former was utilized. Keil uVision5, developed by ARM, was used to program the microcontroller. The conversion process was aided by the built-in Simulink tools, and the harmonic mitigation algorithm was integrated with the fundamental power flow regulator provided by the manufacturer. As detailed in Section III, the proposed algorithm is designed such that the harmonic regulator is layered over the fundamental regulator. To implement the algorithm on the microcontroller, an extra step was included after the reference voltages were calculated, to determine the duty cycles for generating the inverter's switching signals.

Initial trials indicated that the complete Simulink network model was too large for real-time implementation with the available hardware, due to computational constraints. Although the tests could run for a few seconds, equating to a day or two of real-time data, the equipment would eventually

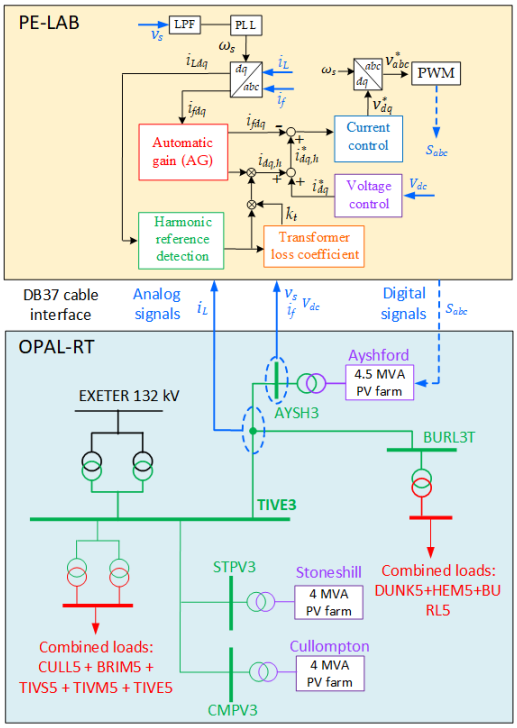

Fig. 11: Schematic representation of the experimental setup

.

trip due to excessive delays causing an unstable output. This issue stemmed from a combination of network components and the substantial size of the data employed. Thus, the network was simplified, ensuring that critical features were maintained to allow comparison with the simulation results. For instance, some lines were represented using pi-sections instead of distributed parameter models, and loads were aggregated, reducing the number of columns in the measurement data matrix. Using pi-section models, the step time for real-time studies was extended to 50 μs, compared to 8 μs in simulation. Furthermore, a 'rate transition' block was added to the model to limit the number of points sent to the workspace, thereby not affecting the waveform visualization while reducing computational demand. The schematic representation of the experimental setup, illustrating the partition between the network model (OPAL-RT), the controller (PE-LAB) and the data exchanged between the two systems is shown in Fig. 11.

Furthermore, the measurement data required adjustment to synchronize the simulation time step with the one used in real-time. The 30-minute SCADA data resolution translated to a simulation step time of 0.1 seconds. Accordingly, the 10-second power quality data resolution corresponded to 0.556 milliseconds in simulation. However, this value was not compatible with RT-LAB, that requires the data sample time to be an integer multiple of the simulation time step. The nearest feasible value was 0.50 milliseconds, yet employing this resolution resulted in a shift in the simulation outputs, as depicted in Fig. 12. This shift became more noticeable over extended simulation durations. To resolve this issue, a decision was made to replicate one PQ measurement point out of every ten, thereby compensating for the time scale compression from

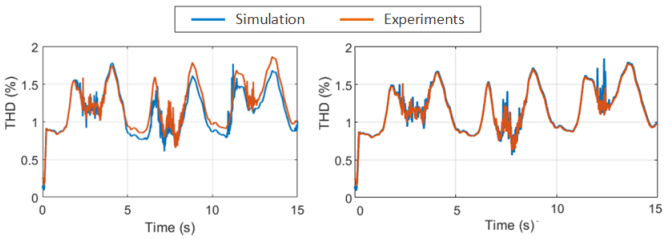

Fig. 12: Results before and after time scale adjustment.

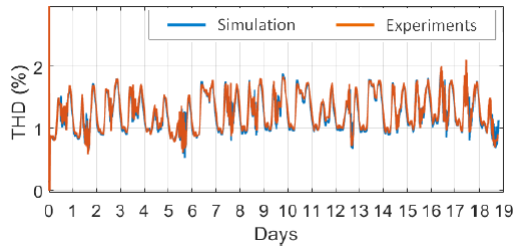

Fig. 13: Comparison of simulation results and measurement results - voltage THD for the observation period.

0.556 milliseconds to 0.5 milliseconds. This decision was based on the observation that the PQ data possess a much higher resolution compared to the SCADA data. Therefore, replicating one point every ten does not significantly deviate from realistic operating conditions. Figure 12 illustrates the comparison over one day and the entire observation period between the original real-time (RT), the modified RT, and the simulation. The modified RT and simulation results were nearly identical.

The THD voltage at TIVE3 is the primary metric used to evaluate the efficiency of the proposed algorithm. For the original network model, the maximum, minimum, and average THD values for the full observation period were recorded at 1.99%, 0.57%, and 1.24%, respectively. The equivalent values with the simplified dynamic model were 1.95%, 0.60%, and 1.25%, respectively, suggesting that the simplified model provides an adequate representation of the original system.

Following this check, the harmonic mitigation algorithm was implemented on the microcontroller to simulate the performance of a single inverter (located at Ayshford PV farm), and to replicate the results achieved in simulation. The inverter current, voltage THD at TIVE3, and transformer losses were observed to be very similar to those obtained in the simulation environment. Specifically, the maximum, minimum, and average THD values were 1.68%, 0.53%, and 1.05% in simulation, and 1.67%, 0.54%, and 1.05% in the HIL tests. These values provided further validation of the developed algorithm.

Figure 13 illustrates the experimental results spanning the entire observation period. This figure shows the THD at TIVE3 for both simulation and experimental tests. The curves closely match each other, thereby confirming the algorithm's effectiveness and proving that experimental verification of large networks is possible with simplified models.

VII. Conclusions

The paper provides a numerical and experimental validation of a control algorithm that utilizes multiple PEIDs as AFs. The proposed algorithm's effectives was highlighted by a comprehensive comparison of the harmonic performance in a real distribution system, both with and without the harmonic mitigation algorithm.

Experimental validation was crucial to evaluate the proposed algorithm's impact. Simplification of the original network model was necessary to achieve real-time operation. One critical aspect was the synchronization of the simulation step time required by the digital simulator with the various sampling times of the SCADA data and the power quality data.

In conclusion, this project showed that HIL is an effective tool for verifying advanced control features and studying the influence of PEIDs on distribution system models. When close comparison of simulation results with experiments is essential, planning a replicable set of simulations with experiments and understanding the limitations of both experimental and computational setups is crucial. For instance, even though a specific set of simulations was planned to be reproduced with HIL experiments from the first phases of the study, adjustments were needed in the experimental phase due to considerations around sampling time and resolution.

Acknowledgement

The Authors acknowledge Ofgem for supporting the research carried out in this project as part of their Network Innovation Allowance (NIA) funding mechanism. The authors would like to thank Yahia Bouzid with OPAL-RT for the support provided during the experimental phase.

Appendix A
List of Abbreviations

AF	Active Filter
AG	Automatic gain
DPF	DIgSILENT PowerFactory
EMT	Electromagnetic transients
HIL	Hardware-in-the-loop
LPF	Low-pass filter
NGED	National Grid Electricity Distribution
NPF	Notch-peak filter
PEID	Power electronics-interfaced devices
PHIL	Power Hardware-in-the-loop
PI	Proportional-integral
PLL	phase-locked loop
PR	Proportional-resonant
PV	Photovoltaic
ZOH	Zero-order hold

References

[1] IEC TR 61000-3-6:2008 Electromagnetic compatibility (EMC)- Part 3-6, "Limits - assessment of emission limits for distorting loads in MV and HV power systems".
[2] IEEE Standard for Harmonic Control in Electric Power Systems, in IEEE Std 519-2022, pp.1-31, 2022.
[3] Engineering Recommendation G5/5, "Harmonic voltage distortion and the connection of harmonic sources and/or resonant plant to transmission systems and distribution networks in the United Kingdom," ENA, London, 2020.

[4] CIGRE Technical Brochure 672, "Power Quality Aspects of Solar Power," JWG C4/C6.29, Paris, December 2016.
[5] K. Al-Haddad, "Power quality issues under constant penetration rate of renewable energy into the electric network," Proceedings of 14th Int. Power Electronics and Motion Control Conf., EPE-PEMC, Ohrid, 2010, pp. S11-39-S11-49.
[6] R. C. Dugan, S. Santoso, M. F. McGranaghan, H. W. Beaty, Electrical Power Systems Quality, McGrawHill Professional, 2002.
[7] M. Diab, M. El-Habrouk, T. H. Abdelhamid and S. Deghedie, "Survey of Active Power Filters Configurations," 2018 IEEE Int. Conf. on Sys., Comp., Autom. and Netw. (ICSCAN), India, 2018, pp. 1-14.
[8] I. Mexis and G. Todeschini, 'Ancillary services provided by battery energy storage systems in the UK: state–of–the–art and future developments', MDPI Energies, Special Issue on Power Electronics and Power Quality, vol 13, no 14, June 2020, pp. 3616-3638.
[9] O. Azofeifa, S. Nigam, O. Ajala, C. Sain, S. Utomi, A. D. Domínguez-Garcia, et al., "Controller hardware-in-the-loop testbed for distributed coordination and control architectures", 2019 North American Power Symposium (NAPS), pp. 1-6, 2019.
[10] S. Yelem, P. Goli, M. Alhashem and S. R. Gampa, "OpenDSS and Typhoon HIL Co-Simulation for Real-Time Evaluation of a Distribution Network," 2023 North American Power Symposium (NAPS), Asheville, NC, USA, 2023, pp. 1-6.
[11] M. A. Ismeil, A. Alfouly, H. S. Hussein and I. Hamdan, "Hardware in the Loop Real-Time Simulation of Improving Hosting Capacity in Photovoltaic Systems Distribution Grid With Passive Filtering Using OPAL-RT," in IEEE Access, vol. 11, pp. 78119-78134, 2023.
[12] K. Prabakar, B. Palmintier, A. Pratt, A. Hariri, I. Mendoza and M. Baggu, "Improving the Performance of Integrated Power-Hardware-in-the-Loop and Quasi-Static Time-Series Simulations," in IEEE Trans. Ind. Electr., vol. 68, no. 11, pp. 10938-10948, Nov. 2021.
[13] D. Çelik, H. Ahmed and M. E. Meral, "Kalman Filter-Based Super-Twisting Sliding Mode Control of Shunt Active Power Filter for Electric Vehicle Charging Station Applications," in IEEE Trans. Pow. Del., vol. 38, no. 2, pp. 1097-1107, April 2023, doi: 10.1109/TPWRD.2022.3206267.
[14] M. C. B. P. Rodrigues, I. D. N. Souza, A. A. Ferreira, P. G. Barbosa and H. A. C. Braga, "Simultaneous active power filter and G2V (or V2G) operation of EV on-board power electronics," IECON 2013 - 39th Annual Conference of the IEEE Industrial Electronics Society, Vienna, Austria, 2013, pp. 4684-4689, doi: 10.1109/IECON.2013.6699891.
[15] L. S. Xavier, A. F. Cupertino and A. P. Heverton, "Ancillary services provided by photovoltaic inverter: single and three phase control strategies," Computers and Electrical Engineering, Vol. 70, pp. 102-121, 2018.
[16] DM. Golla, S. Thangavel, K. Chandrasekaran, S. P. Simon, "Real-Time Implementation of PV Fed Universal Active Power Filter Using CF-SOGI Based IPBT Control Scheme", Electric power systems research 206 (2022).
[17] A. Habash, G. Todeschini, J. Lynch and Z. Emin, "Harmonic Mitigation as Ancillary Service Provided by Multiple Photovoltaic Inverters" 2021 IEEE PES Innovative Smart Grid Technologies Europe (ISGT Europe), Espoo, Finland, 2021, pp. 1-5.
[18] A. Habash, G. Todeschini, J. Lynch and Z. Emin, "Use of PV inverters to mitigate harmonic levels on distribution systems', CIGRE 2022 Symposium, Kyoto, Japan, April 4-7, 2022.
[19] National Grid Electricity Distribution, Harmonic mitigation project website: https://www.nationalgrid.co.uk/innovation/projects/harmonic-mitigation, [Online], Accessed 04/04/2024.
[20] X. Yuan, W. Merk, H. Stemmler and J. Allmeling, "Stationary-frame generalized integrators for current control of active power filters with zero steady-state error for current harmonics of concern under unbalanced and distorted operating conditions," IEEE Trans. Ind. Appl., Vol. 38, No. 2, pp. 523-532, March/April 2002.
[21] A. Vidal, F. Freijedo, A. Yepes, P. Fernandez-Gomesana, J. Malvar, O. Lopez and J. Doval-Gandoy, "Assessment and optimization of the transient response of proportional–resonant current controllers for distributed power generation systems," IEEE Trans. Ind. Electr., Vol. 60, No. 4, pp. 1367-1383, April 2013.
[22] IEEE Std C57.110: Recommended Practice for Establishing Liquid-Immersed and Dry-Type Power and Distribution Transformer Capability When Supplying Nonsinusoidal Load Currents; New York, USA, 2018.
[23] CIGRE Technical Brochure 766, "Network modelling for harmonic studies", JWG C4/B4.38, Paris, April 2019.
[24] G. Nicholson, V. J. Gosbell and A. Parsotam, "Analysis of harmonic distortion levels on a distribution network," Australasian Universities Power Engineering Conference, Perth, Australia, 2007, pp. 1-7.

Grazia Todeschini received her B.Sc. and M.Sc. in Electrical Engineering from the Politecnico di Milano, Italy, and her Ph.D. in Electrical and Computer Engineering from Worcester Polytechnic Institute, in Massachusetts. She was senior consultant with EnerNex, Knoxville, from 2010 to 2013, senior power studies engineer with General Electric in Philadelphia, from 2013 to 2016 and Senior Lecturer at Swansea University from 2016 to 2021. She joined King's College London as a Reader with the Department of Engineering in 2021. She is an IEEE Senior member, secretary of the IEEE Power Quality Subcommittee, IET member, and is part of the steering committee of CIGRE Women in Energy UK. Her research interests include power quality, renewable energy integration, and power system analysis.

Atheer Habash received his B.Sc and M.Sc. degrees in Electrical Engineering from the University of Mosul, Iraq, and his Ph.D. from the University of Sheffield, UK. He has worked as a lecturer at the University of Dohuk, Iraq, and as a research assistant at Swansea University, UK. Currently, he is a lead engineer with GE Vernova. His research and working experience include control and protection of HVDC system, active power filtering, control of permanent magnet machines and drives, and wind power applications.

Jacob Lynch received his BEng degree in Electrical and Electronic Engineering from Cardiff University in 2020. He has since joined National Grid Electricity Distribution where he is currently an Innovation Engineer. His primary focus is on delivering innovative projects that are centered on decarbonization of the distribution network and the wider distribution business. His interests are currently around the use of supercritical fluid technology to extract creosote from redundant wood poles, trialling the viability and impact of heat pump flexibility and assessing the harmonic impact of various Low Carbon Technologies (LCTs) connected to the LV distribution network.

Zia Emin received his B.Sc. from the Middle East Technical University, and M.Sc. and Ph.D. degrees from The University of Manchester. He has worked as a power system engineer specializing in the planning and development of electric power networks, initially with National Grid and later with Parsons Brinckerhoff (later WSP) and PSC. Currently he is working in Electric Power Research Institute (EPRI) as a technical executive. He has been active in many CIGRE (International Council on Large Electric Systems) working groups as member, task force leader and convenor within system technical performance area. He received the CIGRE Technical Committee Award in 2013 and the Distinguished Member Award in 2014. From 2016 to 2022 he was the chairman of CIGRE SC C4 and its Strategic Advisory Group. He was also a member of the CIGRE Technical Council at international level and the past chair at national level (CIGRE-UK). Currently, he is a member of the CIGRE Strategic Advisory Board. He is a Fellow of the Institute of Engineering and Technology (IET - UK), a Senior Member of IEEE, a Distinguished and Honorary Member of CIGRE, a European Engineer, and a Chartered Engineer in the United Kingdom.